New Journal of Physics
The open-access journal for physics

Multimodal x-ray scatter imaging

O Bunk[1,5], M Bech[2,6], T H Jensen[3], R Feidenhans'l[3], T Binderup[4], A Menzel[1] and F Pfeiffer[2,7]

[1] Swiss Light Source, Paul Scherrer Institut, 5232 Villigen PSI, Switzerland
[2] Department Physik (E17), Technische Universität München, James-Franck-Strausse, 85748 Garching, Germany
[3] Niels Bohr Institute, University of Copenhagen, 2100 Copenhagen, Denmark
[4] Rigshospitalet and Faculty of Health Science, University of Copenhagen, 2100 Copenhagen, Denmark
E-mail: oliver.bunk@psi.ch

New Journal of Physics **11** (2009) 123016 (8pp)
Received 29 July 2009
Published 16 December 2009
Online at http://www.njp.org/
doi:10.1088/1367-2630/11/12/123016

Abstract. We describe a small-angle x-ray scattering-based imaging technique that reveals the distribution and orientation of nano-scale structures over extended areas. By combining two measurement and analysis schemes, complementary structural information is available which renders the technique suitable for a broad range of applications, e.g. in materials science and bio-imaging. Through a combination of current techniques and on-line analysis schemes, measurements with a so far unprecedented combination of speed, dynamic range and point density became feasible. This is illustrated by data recorded for a section of a mouse *soleus* muscle visualizing fine muscle and Achilles tendon structures down to the 10 nm range over a 10 mm^2 sample area.

Structures on the nano-scale are of vital importance for the mechanical properties of materials, ranging from bio-medical samples like tissue via polymeric materials to metals and their alloys. Despite its importance there have been very few reports showing nano-scale information for extended objects. High-resolution scanning techniques like scanning transmission x-ray microscopy (STXM) or scanning transmission electron microscopy (STEM) are typically limited to covering small fields of view in the micrometre range on a reasonable timescale or to

[5] Author to whom any correspondence should be addressed.
[6] Until June 2009: University of Copenhagen.
[7] Until February 2009: Paul Scherrer Institut and École Polytechnique Fédérale de Lausanne, 1015 Lausanne, Switzerland.

very thin samples. Full-field two-dimensional (2D) techniques like x-ray microscopy (XRM) or three-dimensional (3D) x-ray micro computed tomography (μCT) and nuclear magnetic resonance (NMR) imaging reveal invaluable information but not down to the nano-scale. Averaging techniques like small-angle x-ray or neutron scattering (SAXS or SANS) access the nano-scale but cannot spatially resolve extended samples. Nevertheless, such techniques are attractive, *inter alia*, for biological studies because of their potential to, e.g. distinguish cancerous from non-cancerous tissue [1]–[3], investigate myelin sheaths of neurons [4, 5], and study dentin [6], bone and cartilage [7, 8]. This has been recognized and accordingly scanning SAXS has been performed, i.e. SAXS measurements at several sample positions [7]–[15]. Here, we report on a combination of SAXS and STXM sensitive to nano-scale structures averaged over a spatial area in the square-micron range. This approach is suitable for imaging samples of several millimetres to centimetres. In principle, the data acquisition and analysis techniques are not novel. However, their combination presented here allows detailed SAXS measurements at a large number of points with high dynamic range and low noise in unprecedented speed. This carries spot-test-like scanning SAXS, as presented in the earlier, ground-breaking work [7]–[15], to microscopy.

Two measurements are undertaken to yield complementary information. First a STXM area scan is performed at reduced incident x-ray intensity and with an area detector. Then an SAXS raster scan is undertaken with the same set-up and speed as for the STXM scan. This combination of techniques coined 'multimodal scatter imaging' has become feasible thanks to a combination of recent technical advances: firstly, pixelated detectors with a high dynamic range, fast readout, no dark counts and no readout noise are now available, such as the single photon counting PILATUS detector [16]–[18]. Secondly, automated data analysis schemes have been developed to analyse for each raster scan several tens of thousands of images of a few megabytes (MB) each, which are sufficiently fast to provide online feedback for the measurements described below. Thirdly, micro-focus options are available at third-generation synchrotron sources, providing the necessary high flux in a small spot for fast scanning measurements.

The set-up for both the STXM and the scanning SAXS measurements is depicted in figure 1. A part of a mouse *soleus* muscle and Achilles tendon was fixated in formalin and mounted in its wet state between two 25 μm thin polyimide foils. This muscle, vital for standing and running, has been chosen as a model system for muscle and tendon tissue. A monochromatic beam of 11.2 keV ($\lambda = 1.107$ Å) was focused to about 20 μm $\times$ 20 μm for the raster scan measurements. For the STXM measurements, the incident intensity of the x-ray beam was attenuated to 0.16% of the full intensity. Two modules of a PILATUS detector, in total about 190 000 pixels, have been used for the measurements. To speed up acquisition, data have been recorded in a continuous line scan mode with the sample moving at constant speed along a line of the 2D raster scan while the detector is continuously recording data. For both the STXM and the SAXS raster scan, the detector was operated with 30 ms exposure time and 10 ms readout time, i.e. with a frame rate of 25 Hz. For the 2D STXM scan, the sample was moved along each line of the scan with a speed of 1 mm s^{-1}, resulting in a signal integrated over 40 μm travel range per exposure. The whole STXM measurement of 101 $\times$ 64 exposures took 9 min. For the SAXS raster scan, half the 'step' size was chosen to cover the same area in 201 $\times$ 127 points with 20 μm 'steps' in both directions. The SAXS data are recorded in a continuous line scan mode as well, i.e. with a 'step' of 20 μm we mean that the sample has been moved by this distance while one detector frame is exposed and read out. A beam-stop was used to protect the

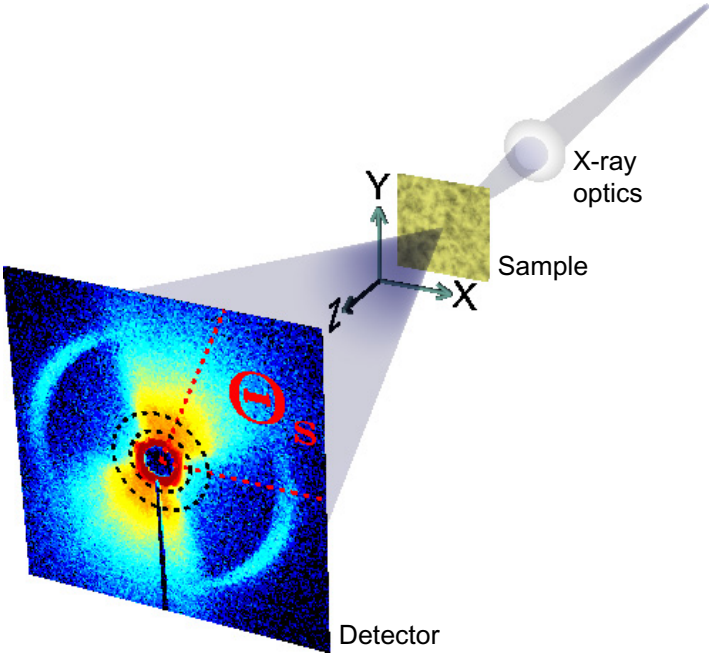

Figure 1. Experimental set-up for both STXM and SAXS measurements (not to scale). The monochromatic x-ray beam is focused on the sample. The sample is raster scanned in the x–y-plane and at each point the scattered intensity is recorded with a fast 2D detector. The sample data recorded with 30 ms exposure time and shown on a logarithmic scale comprise 4.6 out of the six orders of magnitude in photons the detector can count per pixel.

detector and the full available flux was used for the measurements. The whole scanning SAXS measurement took 30 min.

In the STXM raster scan, the x-ray beam is attenuated, refracted and scattered by the sample yielding absorption, differential phase contrast (DPC) and dark field (DF) information. The deflection angles are typically small, in the microradian range and below, but nevertheless it has been demonstrated that segmented [19] and area detectors [20]–[24] are capable of detecting these sub-pixel shifts. These measurements have been taken at the coherent SAXS (cSAXS) beamline at the Swiss Light Source (SLS), where the in-house developed prototype of the commercially available single-photon counting PILATUS 2M detector with 20-bit dynamic range and fast readout is available. Using a pixelated detector has the advantage of calculating all signals in a flexible manner by software [20, 22]. For example, the momentum transfer range for the DF image can be freely chosen.

For the STXM data analysis, the sample transmission at each point T was extracted by comparing the intensities I_s measured with and I_0 without sample, summed over all detector pixels:

$$T = \frac{\sum_{m,n} I_s(x_m, y_n)}{\sum_{m,n} I_0(x_m, y_n)}. \tag{1}$$

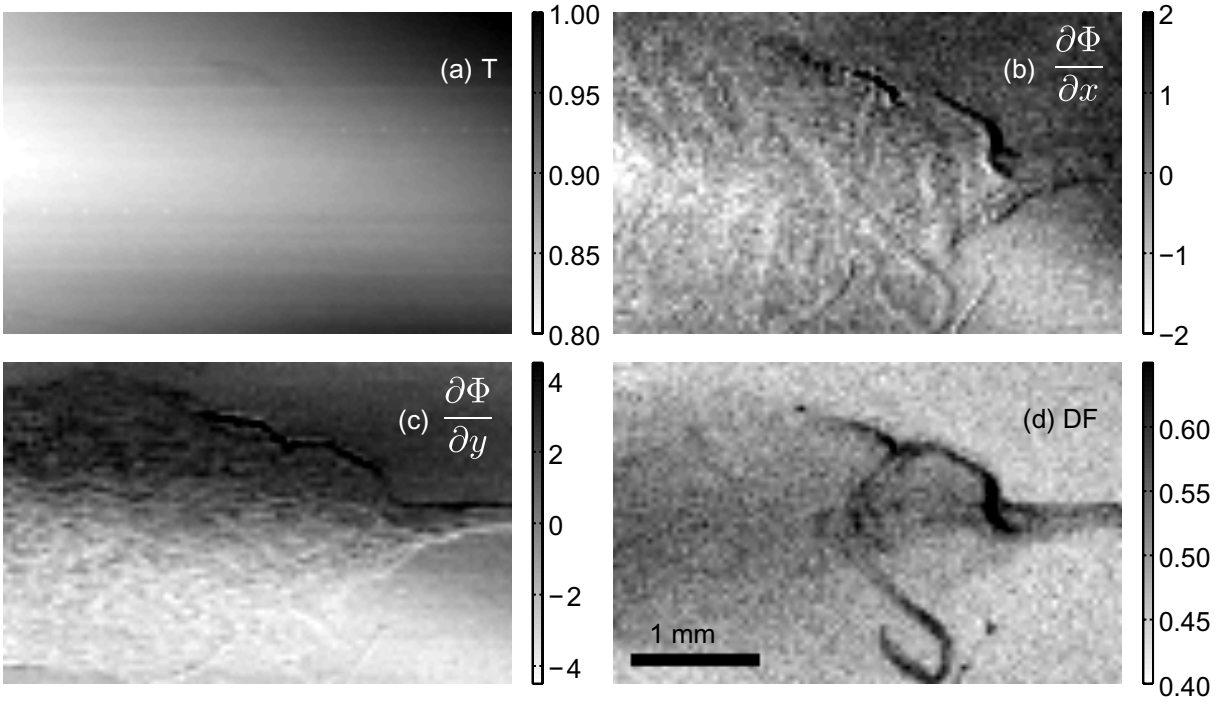

Figure 2. STXM measurement of a mouse *soleus* muscle. Transmission (a), DPC in horizontal (b) and vertical direction (c) in μrad Å^{-1} and a DF image (d) normalized by 10^{-3} times the total detected intensity. The area covered in each plot is 4 mm × 2.5 mm in 101 × 64 'steps' of 40 μm spacing. The measurement took 9 min.

The DPC in the horizontal direction $\partial\Phi/\partial x$, can be extracted by calculating the first moment

$$\frac{\partial\Phi}{\partial x} = c_{\mathrm{s}}\left(\frac{\sum_{m,n}(x_m - x_0)I_{\mathrm{s}}(x_m, y_n)}{\sum_{m,n} I_{\mathrm{s}}(x_m, y_n)} - \frac{\sum_{m,n}(x_m - x_0)I_0(x_m, y_n)}{\sum_{m,n} I_0(x_m, y_n)}\right), \tag{2}$$

whereby the position (x_0, y_0) is that of the undeflected x-ray beam on the detector. The factor $c_{\mathrm{s}} = (a_{\mathrm{d}}/l_{\mathrm{d}})2\pi/\lambda$ converts from pixels of size a_{d} at a sample-to-detector-distance l_{d} to the differential angular units. The DPC $\partial\Phi/\partial y$ is calculated analogously. Finally, a DF can be calculated by summing the detected intensities within a certain radial range R[8]:

$$\mathrm{DF} = \frac{\sum_{r\in R} I_{\mathrm{s}}(r)}{\sum I_{\mathrm{s}}(r)}. \tag{3}$$

While DPC and DF add contrast modalities to the standard transmission imaging, the resolution is still given by the size of the beam that is used for raster scanning the sample. The signals calculated from the STXM data are shown in figure 2. In figure 2(a), one sees that the sample and residual formalin transmission exhibit a smooth slope with no clear features observable at the current resolution, even though the absorption is for biological tissue considerable, up

[8] The radius in pixels r can be converted to the momentum transfer q using the known sample to detector distance l_{d} and the detector pixel size a_{d}: $q = (4\pi/\lambda)\sin(\arctan(ra_{\mathrm{d}}/l_{\mathrm{d}})/2)$. The corresponding structure dimension d in direct space is given as $d = 2\pi/q$.

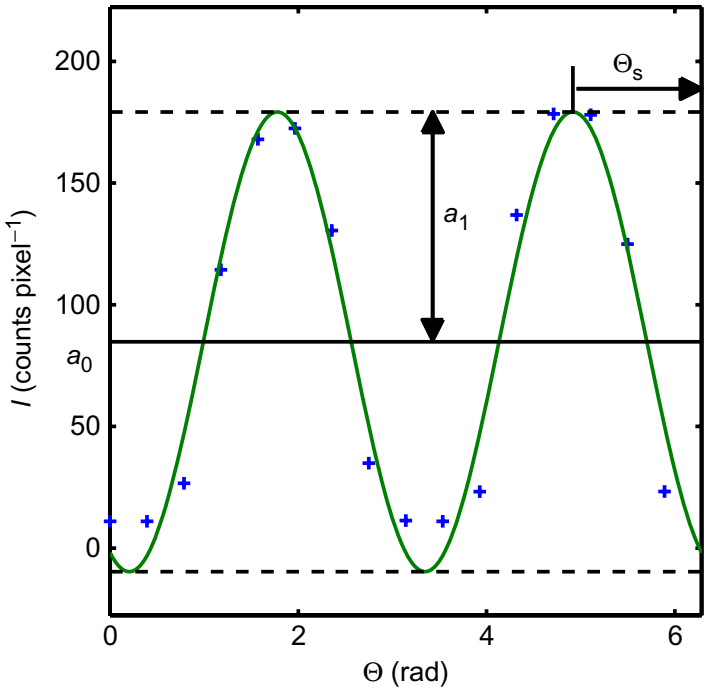

Figure 3. The average intensity in 16 segments of a ring marked with dashed lines in the detector image in figure 1 is plotted using '+' symbols. See the text for further explanations.

to 20%. The DPC depicted in figures 2(b) and (c) allows clear identification of the sample and especially in the DF image in figure 2(d) the Achilles tendon shows up clearly. These results underline the importance of phase contrast for measurements of biological samples.

The STXM measurements provide a fast on-line feedback at moderate x-ray dose on both sample and detector. However, only the SAXS measurements allow access to information on nano-scale structures. It is crucial for these measurements to have a detector with high dynamic range, i.e. six orders of magnitude in photons per pixel and exposure in the present case since SAXS data cover several orders of magnitude in intensity and must be recorded in a single exposure to allow for fast scanning. The scanning speed in turn allows for recording a large number of data points, i.e. high resolution images. For the interpretation, in the present case, of 25 527 SAXS images of 0.8 MB each, clearly an automated analysis scheme is needed, as detailed in the following.

The first step of the SAXS analysis is the azimuthal integration. To capture the asymmetry of the scattering pattern, the summation is performed in $2N_\Theta$ azimuthal segments:

$$I(m_r, n_\Theta) = \frac{1}{A_{m_r,n_\Theta}} \sum_{r\in R(m_r),\Theta\in\theta(n_\Theta)} I(r,\Theta). \tag{4}$$

The intensity is normalized by the number of pixels A in the segment covering the radial range R and the azimuthal range θ and n_Θ and m_r are integer indices. Since the above-described STXM measurements have been performed, an additional normalization by the transmission T is performed to correct for absorption in the sample. An example for the azimuthal integration is shown in figure 3. In the detector image in figure 1, a circular integration area is indicated

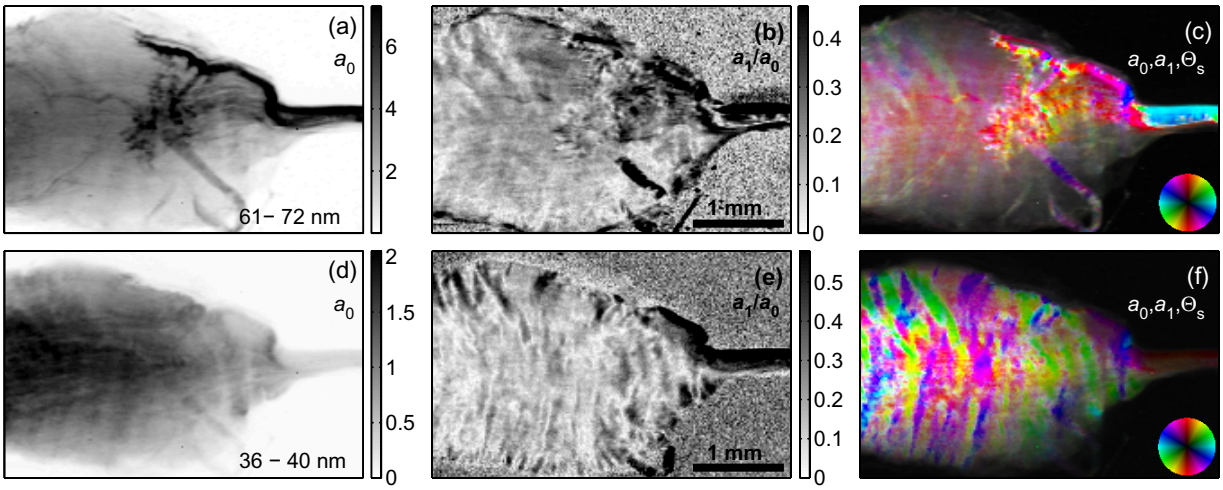

Figure 4. Scanning SAXS measurement of a mouse *soleus* muscle. Structures with dimensions in the specified range have been selected for each row. The average intensity a_0 in counts per pixel scattered from such structures is plotted in the left column. The degree of orientation a_1/a_0 is plotted in the central column. In the right column, the orientation is colour coded according to the colour wheel inset in each plot. In the colour plots, highly oriented material shows up with bright colours, whereas dense material without preferential orientation shows up in white. The measurement comprises 25 527 points and took 30 min.

with dashed lines. This area was divided into $2N_\Theta = 16$ azimuthal segments according to equation (4). The resulting intensity distribution is indicated in figure 3. For typical SAXS samples, i.e. with moderate structural ordering and inversion symmetry of the average structure, this distribution of the integrated intensities is well approximated by a cosine function, as indicated by the solid line in figure 3. The baseline a_0 of this cosine is given by the average scattering within the integration range, whereas the amplitude a_1 is given by the oriented part of it. The degree of orientation can be defined as a_1/a_0. The shift of the cosine function yields the orientation Θ_s of the average scattering. Orientation in this context always means a 2D projection in a plane perpendicular to the x-ray beam. To recover the full 3D information, tomographic measurements under different sample rotation values are required. The above-mentioned inversion symmetry can be utilized to reduce the $2N_\Theta$ data by averaging to N_Θ data points for each integration range. The parameters a_0, a_1 and Θ_s can be extracted from the discrete Fourier transform of the integrated intensities:

$$I(n_\Theta) \approx a_0 + a_1 \cos(2\pi n_\Theta / N_\Theta - \Theta_s). \tag{5}$$

The combination of data reduction via the azimuthal integration according to equation (4) and an analysis scheme based on fast Fourier transforms, equation (5), renders feasible a fast online analysis, which is essential to provide feedback for the measurements.

The result of the described data analysis is shown in figure 4. From the accessible range, approximately 10–380 nm, two ranges of structure dimensions have been chosen: 61–72 nm (figures 4(a)–(c)) and 36–40 nm (figures 4(d)–(f)). The left column shows the distribution of

the average intensity a_0. This can be seen as a density map of structures within the specified range. The central column shows the degree of orientation a_1/a_0. The right column combines the average intensity a_0, the oriented intensity a_1 and the orientation angle Θ_s using a hue-saturation-value representation[9]. Here, the orientation can be directly read from the colour according to the colour wheel inset into each plot. A high density of oriented structures shows up as bright colours, whereas a high density of isotropically scattering structures will show up in white. On average, well below one count per pixel is sufficient for recording a reliable signal since intensity values from several pixels are averaged for obtaining statistically significant data. There are two types of resolution in this scanning SAXS experiment, scanning resolution in direct space and scattering resolution in reciprocal space. The resolution of the raster scanning in a continuous line scan mode is given by the 'step' size, i.e. the distance the sample moves during the exposure, convolved with the size of the beam. In the present case, the sample has been moved by 20 μm during the 30 ms exposure and 10 ms readout time, i.e. the sample moved by 15 μm while the detector was exposing a frame. Convolved with the 20 μm full-width at half-maximum size of the beam the resulting resolution element is 35 μm. Along the 'slow axis', along which no continuous sample movement is performed, step and beam size are matched to 20 μm in the present case. The scattering range and resolution in reciprocal space are given by the angular range over which scattered photons can be reliably detected and the corresponding angular resolution. In the present case with two PILATUS detector modules at a distance of 7150 mm from the sample, the accessible range is approximately 10–380 nm. The structure and orientation on this nanoscale, averaged over the illuminated area of the sample, are detected with each SAXS data frame. Figure 4(c) is a map of mainly the collagen distribution which has a characteristic distance of about 65 nm within the integration range due to the staggered arrangement of tropocollagen fibrils [25, 26]. The Achilles tendon in the right part of the image exhibits the expected orientation of collagen fibres along the tendon, i.e. horizontally. In the muscle, one sees the anchoring of the tendon via a network of fibres. The characteristic distance of 38 nm is attributed to the thin muscle filaments [27, 28]. Correspondingly, the main body of the muscle shows up in the plot of this length scale in figure 4(f). In the 2D measurements performed, so far radiation damage has not been an issue due to the combination of short exposure times and the low absorption of biological tissue.

In summary, multimodal imaging as a combination of STXM and scanning SAXS measurements has been demonstrated using the combination of a novel pixelated x-ray detector, fast Fourier processing schemes for the online analysis of large amounts of data, and an undulator beamline at a third-generation synchrotron. With the example of a mouse *soleus* muscle and Achilles tendon, we illustrated how structural features in the 10–380 nm range can be clearly separated and mapped over extended areas. This new quality of information bridges the gap between high resolution techniques, like electron microscopy operating on thin and small sample areas, and x-ray computed tomography and NMR techniques, operating on larger samples but with lower resolution. We envision further studies on structural changes accompanying myopathies, i.e. muscular diseases. The typical time needed for this kind of measurements places within reach 3D-SAXS tomography as a standard tool for biological and materials science research. This opens up a vast field of applications like investigations of demyelination in brain tissue for research on neurodegenerative diseases, or the effect of orientation on the material properties of cast or fibre reinforced materials.

[9] The hue is given by the orientation, the saturation by a_1 and the value by a_0.

Acknowledgments

This work was performed at the Swiss Light Source, Paul Scherrer Institut, Villigen, Switzerland. We thank Xavier Donath for technical support, Philip R Willmott for fruitful discussions, and the SLS detector group and Dectris for support with the PILATUS detector. FP acknowledges support through the DFG excellence cluster 'Munich Advanced Photonics'.

References

[1] Lewis R A *et al* 2000 *J. Synchrotron Radiat.* **7** 348–52
[2] Fernández M, Keyriläinen J, Serimaa R, Torkkeli M, Karjalainen-Lindsberg M L, Tenhunen M, Thomlinson W, Urban V and Suortti P 2002 *Phys. Med. Biol.* **47** 577–92
[3] Falzon G, Pearson S, Murison R, Hall C, Siu K, Evans A, Rogers K and Lewis R 2006 *Phys. Med. Biol.* **51** 2465–77
[4] Falzon G, Pearson S, Murison R, Hall C, Siu K, Round A, Schültke E, Kaye A H and Lewis R 2007 *Phys. Med. Biol.* **52** 6543–53
[5] De Felici M, Felici R, Ferrero C, Tartari A, Gambaccini M and Finet S 2008 *Phys. Med. Biol.* **53** 5675–88
[6] Kinney J H, Pople J A, Marshall G W and Marshall S J 2001 *Calcif. Tissue Int.* **69** 31–7
[7] Paris O, Žižák I, Lichtenegger H, Roschger P, Klaushofer K and Fratzl P 2000 *Cell. Mol. Biol.* **46** 993–1004
[8] Cedola A, Mastrogiacomo M, Lagomarsino S, Cancedda R, Giannini C, Guagliardi A, Ladisa M, Burghammer M, Rustichelli F and Komlev V 2007 *Spectrochim. Acta* B **62** 642–7
[9] Fratzl P, Jakob H F, Rinnerthaler S, Roschger P and Klaushofer K 1997 *J. Appl. Cryst.* **30** 765–9
[10] Rinnerthaler S, Roschger P, Jakob H F, Nader A, Klaushofer K and Fratzl P 1999 *Calcif. Tissue Int.* **64** 422–9
[11] Lorenz-Haas C, Müller-Buschbaum P, Wunnicke O, Cassignol C, Burghammer M, Riekel C and Stamm M 2003 *Langmuir* **19** 3056–61
[12] Maier G, Wallner G and Fratzl P 2004 *Mater. Res. Soc. Symp. Proc.* **782** 179–85
[13] Schroer C G, Kuhlmann M, Roth S V, Gehrke R, Stribeck N, Almendarez-Camarillo A and Lengeler B 2006 *Appl. Phys. Lett.* **88** 164102
[14] Stribeck N, Almendarez-Camarillo A, Nöchel U, Schroer C, Kuhlmann M, Roth S V, Gehrke R and Bayer R K 2006 *Macromol. Chem. Phys.* **207** 1139–49
[15] Gourrier A, Wagermaier W, Burghammer M, Lammie D, Gupta H S, Fratzl P, Riekel C, Wess T J and Paris P 2007 *J. Appl. Cryst.* **40** s78–82
[16] Kraft P *et al* 2009 *J. Synchrotron Radiat.* **16** 368–75
[17] Henrich B, Bergamaschi A, Broennimann C, Dinapoli R, Eikenberry E F, Johnson I, Kobas M, Kraft P, Mozzanica A and Schmitt B 2009 *Nucl. Instrum. Methods Phys. Res.* A **607** 247–9
[18] Bech M, Bunk O, David C, Kraft P, Brönnimann C, Eikenberry E F and Pfeiffer F 2008 *Appl. Radiat. Isot.* **66** 474–8
[19] Hornberger B *et al* 2008 *J. Synchrotron Radiat.* **15** 355–62
[20] Chapman H N, Jacobsen C and Williams S 1995 *Rev. Sci. Instrum.* **66** 1332–4
[21] Gianoncellia A, Morrison G R, Kaulich B, Bacescu D and Kovac J 2006 *Appl. Phys. Lett.* **89** 251117
[22] Menzel A *et al* 2009 Scanning transmission x-ray microscopy with a fast framing pixel detector (submitted for publication)
[23] Thibault P, Dierolf M, Kewish C M, Menzel M, Bunk O and Pfeiffer F 2009 *Phys. Rev.* A **80** 043813
[24] Menzel A *et al* 2009 Advanced methods in scanning x-ray microscopy *Scanning Microscopy 2009 (Proc. SPIE* vol 7378*)* ed M T Postek, D E Newbury, S F Platek and D C Joy (Bellingham, WA: SPIE) pp 737–80
[25] Buehler J M 2006 *Proc. Natl Acad. Sci. USA* **103** 12285–90
[26] Wilkinson S J and Hukins D W L 1999 *Radiat. Phys. Chem.* **56** 197–204
[27] Yagi N *et al* 1996 *J. Synchrotron Radiat.* **3** 305–12
[28] Sugimoto Y, Takezawa Y, Matsuo T, Ueno Y, Minakata S, Tanaka H and Wakabayashi K 2008 *Biochem. Biophys. Res. Commun.* **369** 100–8